

Hydrothermal Synthesis of N-Doped Graphene/Fe₂O₃ Nanocomposite for Supercapacitors

Nen-Wen Pu^{1,*}, Chun-Yu Chen^{1,2}, Hao-Xiang Qiu¹, Yih-Ming Liu³, Cheng-Han Song¹,
Ming-Hsien Lin³, Ming-Der Ger^{3,*}

¹ Department of Photonics Engineering, Yuan Ze University, Zhongli, Taoyuan 320, Taiwan

² Chemical System Research Division, National Chung Shan Institute of Science and Technology, Longtan, Taoyuan 325, Taiwan

³ Department of Chemical & Materials Engineering, Chung Cheng Institute of Technology, National Defense University, Dasi, Taoyuan 335, Taiwan

*E-mail: nwpuccit@saturn.yzu.edu.tw; mingderger@gmail.com

Received: 17 March 2018 / Accepted: 20 April 2018 / Published: 5 June 2018

A facile hydrothermal method for synthesizing N-doped graphene/Fe₂O₃ nanocomposite and its application to supercapacitors is demonstrated. The combination of large theoretical specific conductance of Fe₂O₃ with the high conductivity of N-doped graphene resulted in excellent capacitance values and high-rate performance. N-doped graphene offered lower charge transfer resistance as well as better wettability between the graphene and the electrolyte. This increased the ion diffusion rate and accessible surface area. Samples prepared with and without N-doping were characterized and their electrochemical performances compared. N-doping increased the specific capacitance at 1 A/g from 543 F/g to 698 F/g. A capacitance as high as 354 F/g was retained when the current density was raised to 20 A/g.

Keywords: graphene, nitrogen doping, hydrothermal, iron oxide, supercapacitor.

1. INTRODUCTION

As a competing energy-storage system to rechargeable batteries, supercapacitors (SCs) offer considerably higher power density and charging speed. In addition, SCs also have high coulombic efficiency, long cycle life, and wide working temperature range [1,2]. Two types of SCs based on different charge storage mechanisms [3,4] are commonly used: (1) electric double-layer capacitors (EDLCs), which store ions at the interface between electrode and electrolyte by means of a physical interaction, and (2) faradaic capacitors (pseudocapacitors), which store energy through redox reactions between the electrode materials during charge/discharge processes [5].

Graphene, or reduced graphene oxide (RGO), is a two-dimensional structure that is only one or few atomic layers thick [6,7]. It is considered an excellent material for SC electrodes because of its exceptionally high specific surface area, good conductivity, and many other desirable chemical and physical properties. The specific surface area of graphene has a significant effect on an SC's capacitance. Unfortunately, this value often degrades severely due to the restacking of exfoliated graphene sheets. The issue of how to overcome the restacking tendency of graphene is consequently of utmost importance for SC applications.

In recent years, graphene/metal oxide composites have been reported to exhibit anti-restacking capability due to the fact that metal oxide particles grown on the basal plane of graphene can prevent neighboring graphene flakes from face-to-face restacking. In addition, many researchers have found that metal oxides (e.g. NiO [8], Ni(OH)₂ [9], MnO₂ [10,11], and Fe₃O₄ [12-14]), or conductive polymers [15-18] can increase the capacitance by way of redox reactions with the electrolyte. Electrochemical tests have revealed that, the combination of the pseudo-capacitance offered by metal oxides or conductive polymers with the large EDLC effect of graphene can result in significantly enhanced electrochemical performance. Among transition metal oxides, iron oxide has the advantages of non-toxicity, low cost, high chemical and thermal stability, corrosion resistance, natural abundance. Thus it has a wide range of applications, such as gas sensors, optical devices, and electromagnetic devices [19-21]. Theoretically, α -Fe₂O₃ is known to have a capacitance as high as 3625 F/g, deriving from the pseudo-capacitance effect during the reversible redox reaction: $\text{Fe}^{3+} \leftrightarrow \text{Fe}^{2+}$ [22].

Despite the many advantages of iron oxide, it has a major drawback, namely, poor conductivity. This results in deteriorated performance at high current densities due to high charge transfer resistance. This can be overcome by combining iron oxide and graphene to form a composite material: the high conductivity of graphene can improve the charge transfer rate at the electrodes [23-25]. In recent years, in order to improve the properties of graphene, many researchers have doped graphene with nitrogen atoms [26,27]. Apart from increasing the conductivity of graphene, N-doping improves the wetting of graphene in the electrolyte, thereby increasing the ion transport efficiency, capacitance value, and electrochemical stability.

Here we present a simple, low-cost hydrothermal method for producing N-doped graphene/Fe₂O₃ composites. These composites possess the following desirable properties for SC applications. Firstly, Fe₂O₃ offers an excellent specific capacity (3625 F/g theoretically). Secondly, N-doping raises graphene's conductivity at the electrode. Thirdly, N-doping improves the wettability between graphene and the electrolyte, thereby greatly promoting ion diffusion.

2. EXPERIMENTAL DETAILS

2.1. Preparation of graphene/iron oxide composites

Graphite oxide (GO) was prepared following the Staudenmaier method [28]. Sulfuric acid (105 ml) was mixed with nitric acid (54 ml) before being stirred for 15 min in an ice bath, followed by addition of natural graphite powder (6 g). After stirring for 15 min, the mixture was stirred for 15 min

and potassium perchlorate (66 g) slowly added (to avoid strong reactions). This was followed by 96 h of continuous stirring in the ice bath. After the addition of 5 L of deionized water, the mixture was filtered and then washed with 5% HCl to remove the SO_4^{2-} ions. The solution was then repeatedly washed with deionized (DI) water until the pH became neutral. Finally, GO was obtained by filtering and drying of the solution.

0.3 g of the synthesized GO along with 1.05 g of ferric chloride were dissolved in 150 ml of alcohol and ultrasonicated for 10 min. After this 3.885 g of sodium acetate was added to the solution, which was mixed by a magnetic stirrer at 500 rpm, and then autoclaved at 180°C for 12 hours. After the reaction finished, the solution was vacuum-filtrated. Finally, the filtrate was washed with DI water to neutralize its pH, and dried at 80°C in an oven for 12 hours to obtain the graphene/iron oxide composite (RGO/ Fe_2O_3) powder.

2.2. Synthesis of N-doped RGO/ Fe_2O_3 composites

0.4 g of RGO/ Fe_2O_3 powder was added in 100 ml of DI water, and then ultrasonicated for 15 min. 2 g of melamine powder was added to the mixture, which was stirred at 500 rpm to achieve uniform dispersion before heating in an autoclave at 180°C for 12 hours. Subsequently, the solution was vacuum-filtered, and its pH was neutralized by washing with DI water. Finally, the solution was dried in an oven overnight at temperature of 80°C , generating graphene/iron oxide (N-RGO/ Fe_2O_3) powder.

2.3. Material characterization and electrochemical measurements

X-ray diffractometry (XRD, Bruker, D2 Phaser) was employed to determine the crystal structure of the synthesized nanocomposite samples before observing the surface morphology with a scanning electron microscope (SEM, JEOL, JSM-6500). A transmission electron microscope (TEM) (JEOL, JEM-2000 EX II) was used in examining the high-resolution morphology. X-ray photoelectron spectra (XPS) of the nanocomposites were measured with a high-resolution ULVAC-PHI XPS spectrometer (Model: PHI Quantera SXM/Auger: AES 650) in order to verify the success of N-doping.

All three-electrode electrochemical analysis experiments were performed with a potentiostat (BioLogic, SP-150). The working electrode was prepared by first creating an electrode slurry by dispersing the prepared nanocomposites (80 wt.%) uniformly in N-Methyl-2-pyrrolidone (NMP) along with carbon black (10 wt.%) and polyvinylidene fluoride (PVDF, 10 wt.%). The slurry was then immersion-coated onto a Ni foam ($1 \times 1 \text{ cm}^2$), and then baked in a vacuum oven (90°C) overnight. The loaded Ni foam was then compressed under a pressure of 150 kgf/cm^2 to obtain the working electrode.

The counter and reference electrodes were, respectively, a platinum foil and Ag/AgCl. The electrolyte was 1 M KOH aqueous solution. Cyclic voltammetry (CV) and galvanostatic charge/discharge (GC) electrochemical tests were conducted at room temperature with a voltage range between -1.2 and 0 V. From the CV and GC curves, the specific capacitance (C_s , in F/g) was calculated. The performance at various scan rates and current densities were studied in order to

evaluate the rate capabilities of the SCs. Finally, to obtain the parameters of the equivalent circuit elements, electrochemical impedance spectroscopy (EIS) measurements were carried out with alternating-circuit (AC) frequency scanning between 10 mHz and 100 kHz.

3. RESULTS AND DISCUSSION

Fig. 1 displays the XRD results for RGO/Fe₂O₃ and N-RGO/Fe₂O₃ powders. The diffraction peaks for α -Fe₂O₃ (JCPDS No.88-2359) are clearly seen for both samples. No apparent differences were observed between the two. The graphite (002) peak at 26° was not observable, indicating a high degree of exfoliation in both of the graphene nanocomposites.

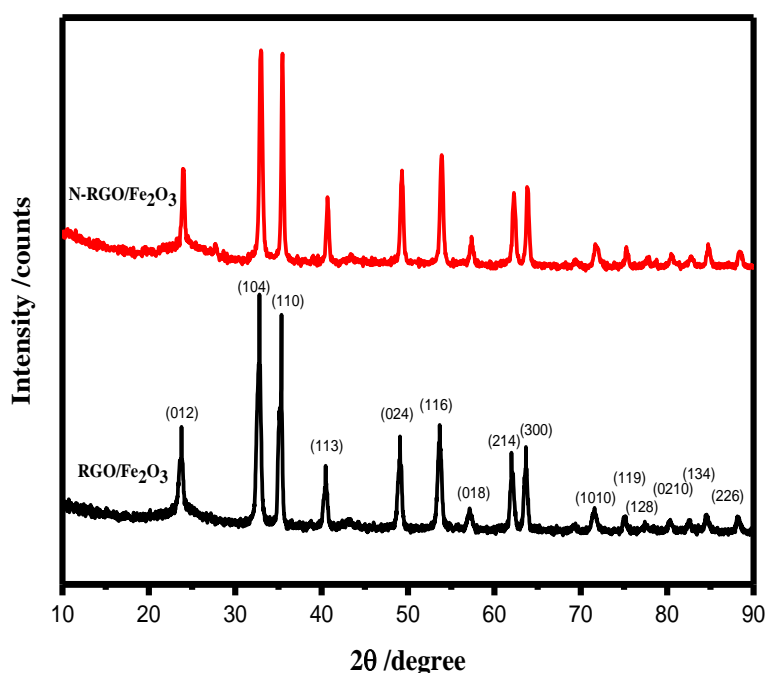


Figure 1. XRD results of N-RGO/Fe₂O₃ and RGO/Fe₂O₃ composites.

The surface morphology of the nanocomposites was observed with SEM. Figs. 2(a) and (c) show the electron micrographs of the synthesized RGO/Fe₂O₃ and N-RGO/Fe₂O₃, respectively, while Figs. 2(b) and (d) show the high-magnification counterparts. The surface of RGO was densely covered with iron oxide nanoparticles in both samples. There are no distinct differences in their morphology. The high-magnification SEM images reveal that the iron oxide particles had a disk shape with diameters ranging from 50 to 100 nm. More detailed surface morphology was observed with TEM. Figs. 2(e) and (f) show, respectively, the TEM micrographs of N-RGO/Fe₂O₃ with low and high magnifications. They reveal that the RGO was quite thin and covered uniformly and densely with Fe₂O₃ nanoparticles.

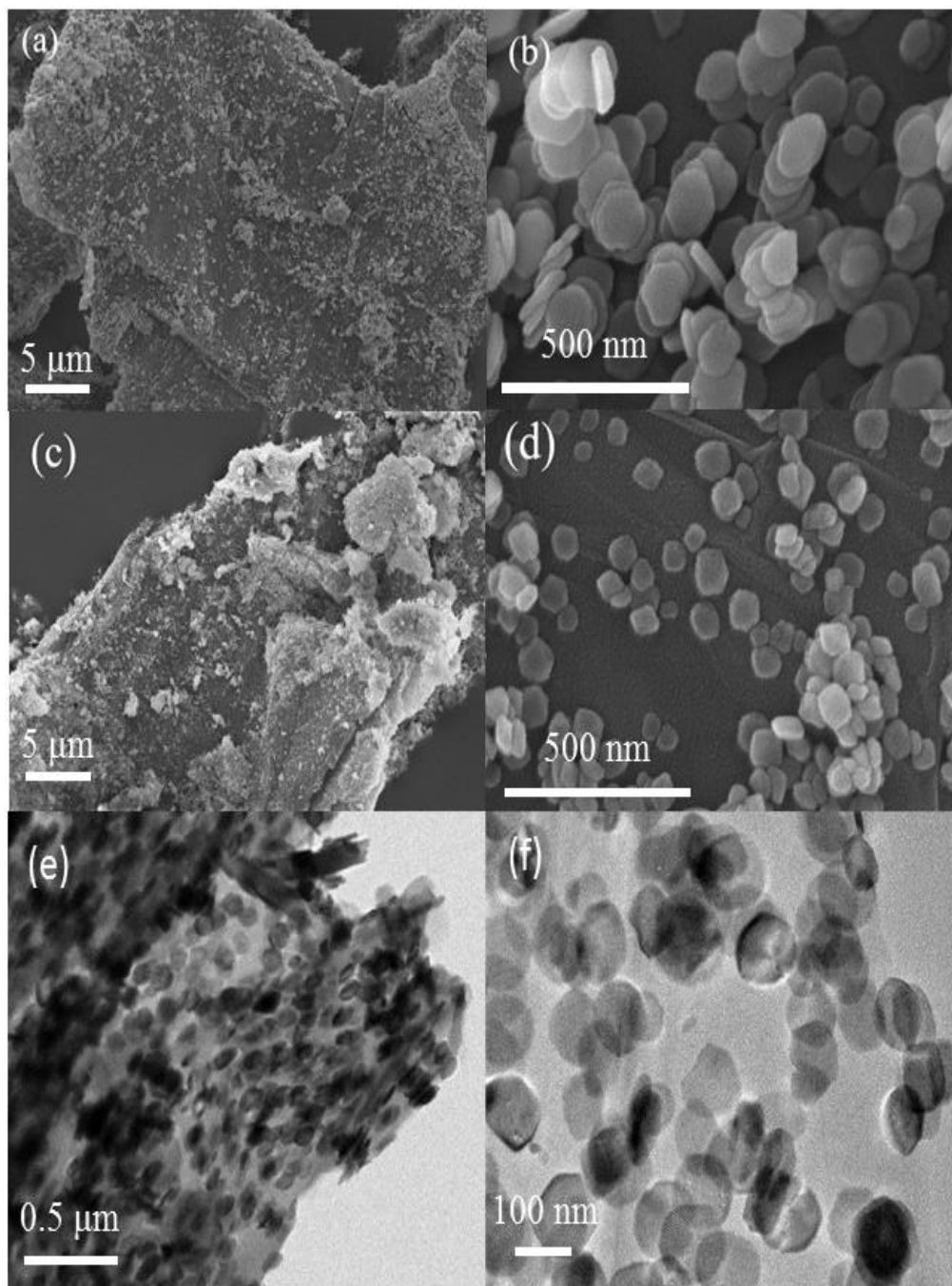


Figure 2. SEM micrographs of (a, b) RGO/Fe₂O₃ and (c, d) N-RGO/Fe₂O₃ composites. (e, f) TEM micrographs of N-RGO/Fe₂O₃.

In order to understand in detail the composition and electronic structure of the RGO/Fe₂O₃ and N-RGO/Fe₂O₃ composites. XPS analysis was performed. As depicted in Fig. 3 (a), XPS shows that both composites contain iron, carbon, and oxygen, but nitrogen was only found in N-RGO/Fe₂O₃. Thus we verified that N-doping of RGO with melamine was successfully achieved. The content of N was estimated to be about 21.5 at.%. Fig 3 (b) presents the C1s electron spectrum for N-RGO/Fe₂O₃. It can be deconvoluted into five peaks: C=C/C-C (284.7 eV), C-N (285.4 eV), C-O (286.5 eV), C=O (288.5 eV), and O-C=O (289.4 eV) [29,30].

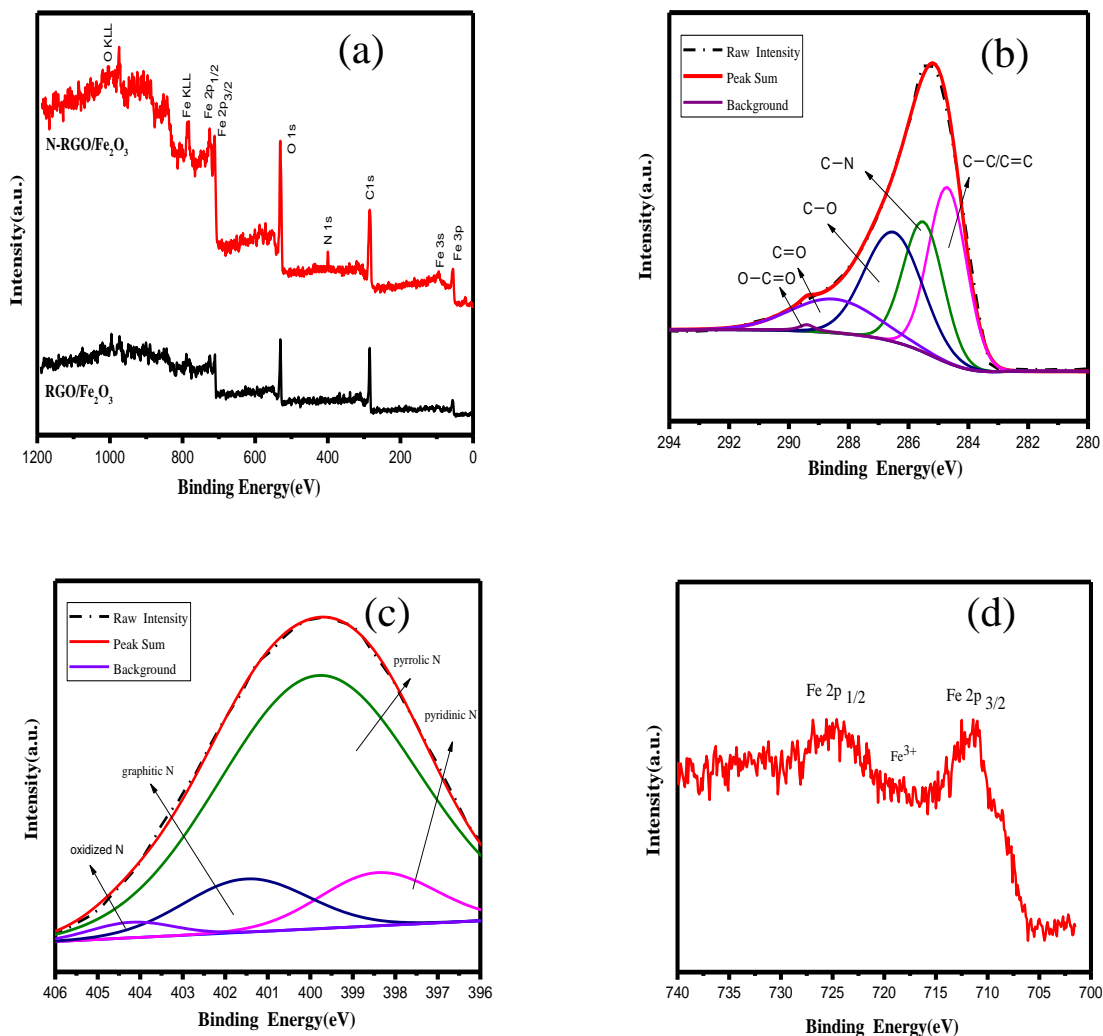
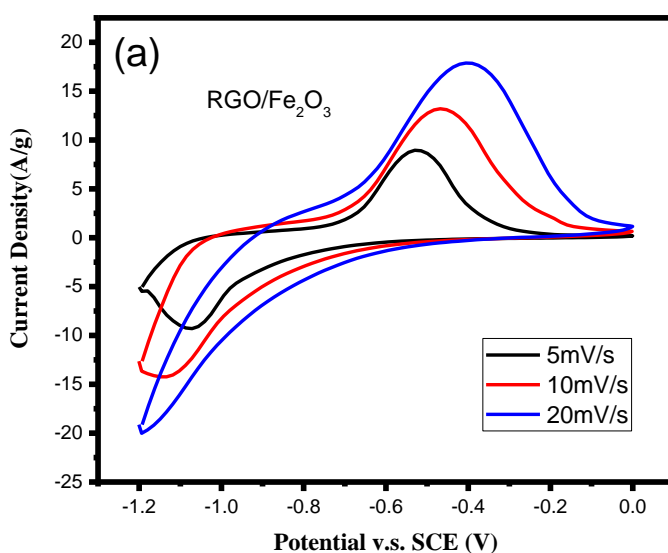


Figure 3. (a) XPS analysis for N-RGO/Fe₂O₃ and RGO/Fe₂O₃. (b) C 1s (deconvoluted), (c) N 1s (deconvoluted), and (d) Fe 2p lines of N-RGO/Fe₂O₃.

To study the bonding of N atoms, the N 1s spectrum was inspected. Deconvolution indicated that 4 peaks were present, as revealed in Fig. 3 (c): pyridinic N at 398.4 eV, pyrrolic N at 399.7 eV, graphitic N at 401.5 eV, and oxidized N at 404.2 eV [29]. Clearly pyrrolic N was the dominant dopant atom in our sample. It is known that pyrrolic N is a good electron donor for graphene because it offers high mobility [29], which facilitates electron-transfer reactions and thus enhances the performance of SCs [26,27,31]. Additionally, pyridinic N can also serve as an electron donor [31-33]. Consequently, N-doping improves graphene's conductivity and electrochemical activity, leading to better high-rate performance of SCs [34]. XPS also showed two Fe 2p peaks at 710.9 and 724.5 eV (see Fig. 3(d)), which are attributed to 2p_{3/2} and 2p_{1/2} of Fe³⁺, respectively [29]. This offers another piece of evidence for the successful synthesis of Fe₂O₃ nanoparticles on N-RGO sheets.

Electrochemical analysis was carried out for the two nanocomposite materials to probe the influence of N-doping on SC's electrochemical properties. Electrodes made of RGO/Fe₂O₃ and N-RGO/Fe₂O₃ were prepared separately for testing. The CV results are shown in Fig. 4. All curves differ significantly from the approximately rectangular profile seen for pure EDLCs (the result of the physical processes of electrostatic adsorption and desorption). They clearly exhibit Faraday pseudocapacitance effects, which are offered by the redox chemical reactions of the iron oxide nanoparticles. The CV curves reveal a reduction reaction at ~ -1.0 V and an oxidation reaction at ~ -0.7 V. We attribute this to a reversible reaction between Fe³⁺ and Fe²⁺ [29]. The large redox peaks indicate that the specific capacitance is mainly due to the pseudocapacitance effect of iron oxide.

Fig. 5(a) displays the GC test results for N-RGO/Fe₂O₃ for current densities varying from 1 to 20 A/g. All of the curves deviate considerably from ideal quasi-isosceles triangles found in pure EDLCs. Consistent with CV, GC tests indicate that most of the energy was stored by means of the pseudocapacitance effect, i.e., redox reactions of iron oxide. The curves reveal that the redox reactions occur at ~ -0.7 and -1.0 V, in agreement with the CV measurements. The specific capacitances (calculated from the GC tests) for RGO/Fe₂O₃ and N-RGO/Fe₂O₃ as functions of current density are compared in Fig. 5(b). N-RGO/Fe₂O₃ shows consistently higher capacitance than RGO/Fe₂O₃ at all current density levels. At the lowest current density (1 A/g), the former offered a capacitance as high as 698 F/g, while the latter gave only 543 F/g. This confirms that N-doping is an effectively way to raise the capacitance of RGO-based SCs. When the current density was drastically increased to 20 A/g, the specific capacitance of N-RGO/Fe₂O₃ fell only to 354 F/g. This corresponds to an 85%-improvement compared to RGO/Fe₂O₃. This performance indicated that N-doping has the benefit of enhancing the capacitance retention of RGO at large currents. We ascribe these overall improvements in specific capacitance values as well as retention ratios by way of N-doping to better conductivity as well as enhanced wettability, which facilitates ion transport and increased accessible surface area within the electrode material.



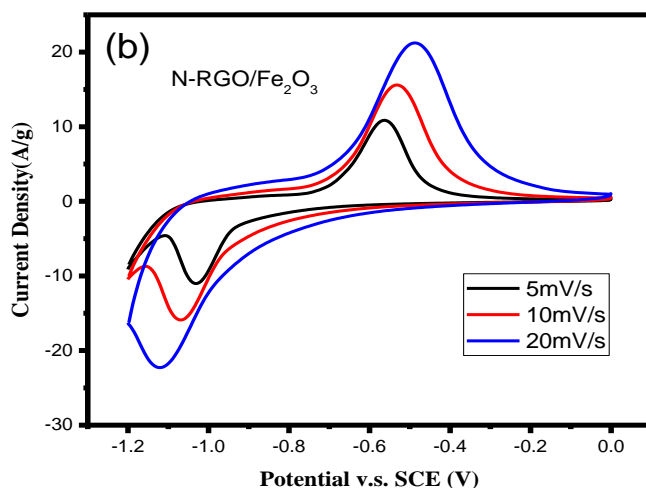


Figure 4. CV curves at scan rates of 5, 10, and 20 mV/s for (a) RGO/Fe₂O₃ and (b) N-RGO/Fe₂O₃.

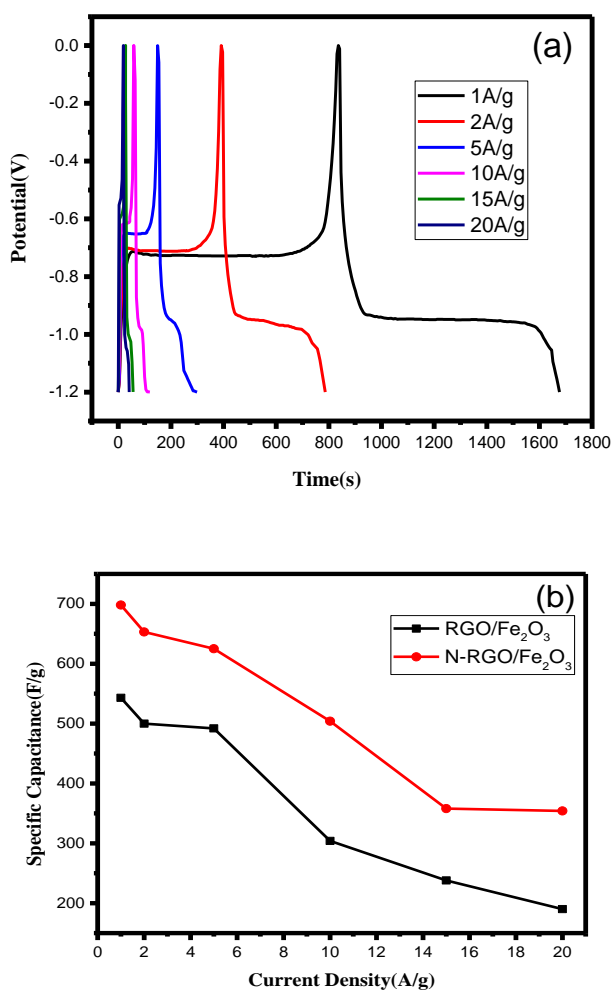


Figure 5. (a) GC measurement results at current densities of 1 to 20 A/g for N-RGO/Fe₂O₃ electrode. (b) Specific capacitance vs. current density for N-RGO/Fe₂O₃ and RGO/Fe₂O₃.

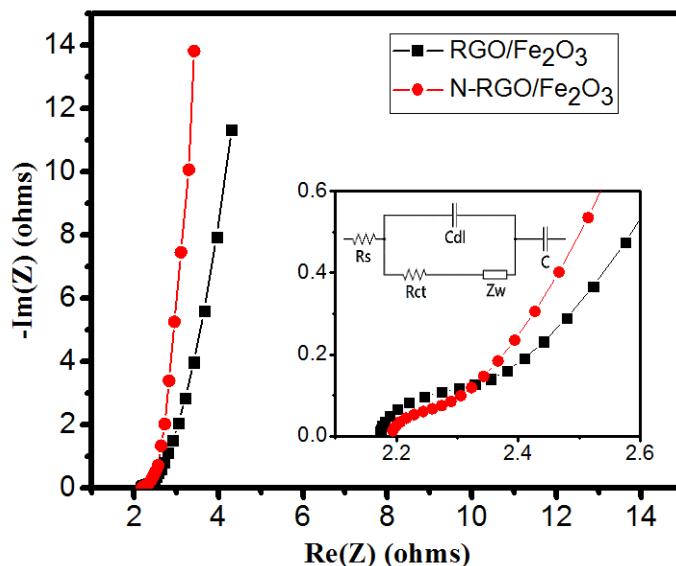


Figure 6. EIS characterization of RGO/Fe₂O₃ (black square) and N-RGO/Fe₂O₃ (red circle) and equivalent circuit.

To further understand the charge transport characteristics, EIS tests were carried out on both electrodes over a frequency range from 100 kHz to 10 mHz. Figure 6 shows the real and imaginary parts of the AC impedance as the x - and y -axes on the Nyquist plot. The x -axis intercept on the left (i.e., the high-frequency region) represents the internal impedance, R_s . This comprises the resistances of the active material, the electrolyte, and the contact resistance (at the interface between the active material and the collector) [35]. The two curves have very close R_s values, indicating that the overall resistances for the two electrodes are similar. The oblique line at the low frequency end (on the right) suggests a diffusion-controlled kinetic process in the electrode. The larger slope observed for the N-RGO/Fe₂O₃ electrode indicates that it has faster ion diffusion and consequently a higher formation rate of EDL than the RGO/Fe₂O₃ electrode. The arc in between the two frequency extremities is associated with another kind of resistance--the charge transfer resistance (R_{ct}). R_{ct} is often ascribed to the Faraday reaction occurring at the contact with electrolyte and is a limiting factor for the specific power of the supercapacitor. The smaller arc in the EIS plot of N-RGO/Fe₂O₃ implies a smaller R_{ct} . The R_{ct} values extracted from equivalent circuit simulation for N-RGO/Fe₂O₃ and RGO/Fe₂O₃ were 0.08 and 0.23 Ω , respectively. This confirms that nitrogen doping effectively reduces R_{ct} due to the higher conductivity of graphene sheets as well as the improved wettability between the graphene surface and the electrolyte. The lower R_{ct} results in the higher specific power of the N-RGO/Fe₂O₃ electrode.

Finally, the N-RGO/Fe₂O₃ supercapacitor was subjected to a cycle life test. Fig. 7 displays its capacitance retention behaviour over 3000 cycles of charge and discharge (at 1 A/g). After 3000 cycles, the capacitance value decayed by 45%, which was expected because the capacitance mainly came from the Faraday reaction in Fe₂O₃ rather than from EDLC. However, due to the high initial specific capacitance, a large value of 384 F/g was still retained after 3000 cycles.

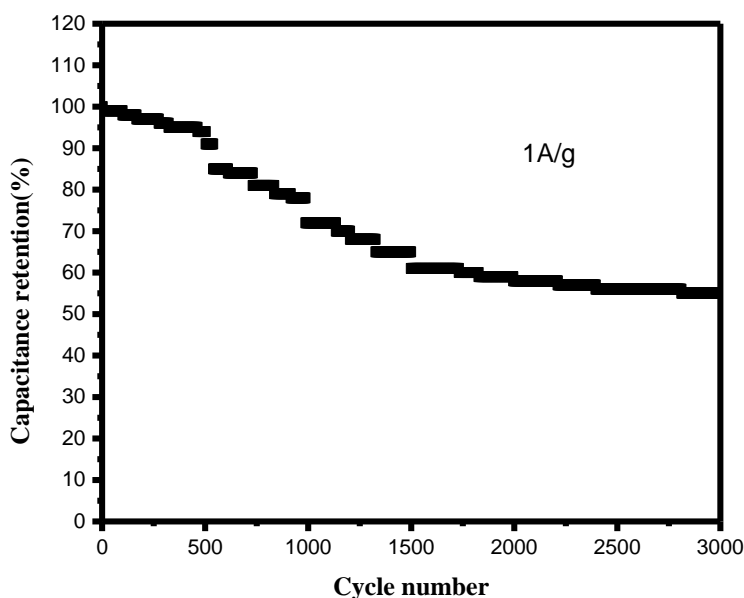


Figure 7. Cycle performance for N-RGO/Fe₂O₃ at 1 A/g for 3000 cycles.

Table 1 compares the supercapacitor properties of the investigated composite with those of similar composites reported in the literature. It shows that our simple method gives excellent results in comparison with other methods.

Table 1. Supercapacitor properties of investigated composite and similar composites.

Composite type	Electrolyte Voltage window	Capacitance (F/g)	Capacitance retention	Ref.
Fe ₂ O ₃ NDs@NG- 0.75	2 M KOH -1.0 to 0 V	274 at 1 A/g 140 at 50 A/g	100,000 cycles 75.3% at 5 A/g	[29]
Fe ₂ O ₃ /N-rGO	1 M KOH -1.1 to -0.7 V	618 at 0.5 A/g 350 at 10 A/g	5,000 cycles 56.7% at 4 A/g	[30]
N-rGO/Fe ₂ O ₃	1 M KOH -1 to -0 V	268.4 at 2 A/g 137 at 5 A/g	2,000 cycles 4.21% at 3 A/g	[36]
NGFeCs	1 M Na ₂ SO ₄ -1.1 to -0.1 V	260.1 at 2 A/g 110.4 at 7 A/g	1,000 cycles 82.5% at 2 A/g	[37]
NGHs	6 M KOH -1 to -0 V	326 at 1 A/g 308 at 3 A/g	1,200 cycles 92% at 3 A/g	[38]
N-RGO/Fe ₂ O ₃	1 M KOH -1.2 to 0 V	698 at 1 A/g 354 at 20 A/g	3,000 cycles 55% at 4 A/g	This work

4. CONCLUSIONS

N-doped graphene/Fe₂O₃ composites via a simple hydrothermal method using melamine as the nitrogen source were successfully synthesised. As the active material of an SC, in addition to reducing charge transfer resistance, N-doping on the graphene surface improved the wettability between electrode and electrolyte. The latter facilitates ion diffusion during the charge/discharge process at high current and increases the accessible surface area of the active material. The incorporation of Fe₂O₃ effectively enhanced the capacitance values of the SCs due to its high specific capacitance. The SC based on the N-RGO/Fe₂O₃ electrode exhibited excellent specific capacitance values at low and high current densities: 698 (1 A/g) and 354 (20 A/g) F/g, respectively. Cycle life testing showed good retention of capacitance. In summary, combining the advantages of N-doped graphene with the high specific capacitance of Fe₂O₃ leads to the superior performance. This will be useful for future applications of SCs.

References

1. C. Largeot, C. Portet, J. Chmiola, P. L. Taberna, Y. Gogotsi and P. Simon, *J. Am. Chem. Soc.*, 130 (2008) 2730.
2. G. Wang, L. Zhang and J. Zhang, *Chem. Soc. Rev.*, 41 (2012) 797.
3. B. E. Conway, V. Birss and J. Wojtowicz, *J. Power Sources*, 66 (1997) 1.
4. Y. Gao, Y. S. Zhou, M. Qian, H. M. Li, J. Redepenning, L. S. Fan, X. N. He, W. Xiong, X. Huang, M. Majhouri-Samani, L. Jiang and Y. F. Lu, *RSC Adv.*, 3 (2013) 20613.
5. Y. Wang and Y. Xia, *Adv. Mater.*, 25 (2013) 5336.
6. C. Soldano, A. Mahmood, E. Dujardin, *Carbon*, 48 (2010) 2127.
7. M. Ioniță, G. M. Vlăsceanu, A. A. Watzlawek, S. I. Voicu, J. S. Burns and H. Iovu, *Composites Part B*, 121 (2017) 34.
8. Y. Z. Zheng, H. Y. Ding and M. L. Zhang, *Mater. Res. Bull.*, 44 (2009) 403.
9. X. Wang, J. Liu, Y. Wang, C. Zhao and W. Zheng, *Mater. Res. Bull.*, 52 (2014) 89.
10. N. Tang, X. Tian, C. Yang and Z. Pi, *Mater. Res. Bull.*, 44 (2009) 2062.
11. J. Yan, T. Wei, J. Cheng, Z. Fan and M. Zhang, *Mater. Res. Bull.*, 45 (2010) 210.
12. T. Qi, J. Jiang, H. Chen, H. Wan, L. Miao and L. Zhang, *Electrochim. Acta*, 114 (2013) 674.
13. Q. Wang, L. Jiao, H. Du, Y. Wang and H. Yuan, *J. Power Sources*, 245 (2014) 101.
14. W. Shi, J. Zhu, D. H. Sim, Y. Y. Tay, Z. Lu, X. Zhang, Y. Sharma, M. Srinivasan, H. Zhang, H. H. Hng and Q. Yan, *J. Mater. Chem.*, 21 (2011) 3422.
15. J. Yan, T. Wei, Z. Fan, W. Qian, M. Zhang, X. Shen and F. We, *J. Power Sources*, 195 (2010) 3041.
16. H. Wang, L. Ma, M. Gan, T. Zhou, X. Sun, W. Dai, H. Wang and S. Wang, *Composites Part B*, 92 (2016) 405.
17. N. Parveen, N. Mahato, M. O. Ansari and M. H. Cho, *Composites Part B*, 87 (2016) 281.
18. A. Moyseowicz, A. Śliwak, E. Miniach and G. Gryglewicz, *Composites Part B*, 109 (2017) 23.
19. K. Kanie and A. Muramatsu, *J. Am. Chem. Soc.*, 127 (2005) 11578.
20. P. Chauhan, S. Annapoorni and S. K. Trikha, *Thin Solid Films*, 346 (1999) 266.
21. T. Ohmori, H. Takahashi, H. Mametsuka and E. Suzuki, *Phys. Chem. Chem. Phys.*, 2 (2000) 3519.
22. Y. Gao, D. Wu, T. Wang, D. Jia, W. Xia, Y. Lv, Y. Cao, Y. Tan and P. Liu, *Electrochim. Acta*, 191 (2016) 275.
23. H. Wang, Z. Xu, H. Yi, H. Wei, Z. Guo and X. Wang, *Nano Energy*, 7 (2014) 86.

24. J. Chen, J. Xu, S. Zhou, N. Zhao, C. P. Wong, *Nano Energy*, 15 (2015) 719.
25. H. Quan, B. Cheng, Y. Xiao and S. Lei, *Chem. Eng. J.*, 286 (2016) 165.
26. H. M. Jeong, J. W. Lee, W. H. Shin, Y. J. Choi, H. J. Shin, J. K. Kang and J. W. Choi, *Nano Lett.*, 11 (2011) 2472.
27. Y. Qiu, X. Zhang and S. Yang, *Phys. Chem. Chem. Phys.*, 13 (2011) 12554.
28. H. C. Schniepp, J. L. Li, M. J. McAllister and S. Hiroaki, *Phys. Chem. Lett.*, 110 (2006) 8535.
29. L. Liu, J. Lang, P. Zhang, B. Hu and X. Yan, *ACS Appl. Mater. Interfaces*, 8 (2016) 9335.
30. Z. Ma, X. Huang, S. Dou, J. Wu and S. Wang, *J. Phys. Chem. C*, 118, (2014) 17231.
31. S. Yang, X. Song, P. Zhang and L. Gao, *ACS Appl. Mater. Interfaces*, 5 (2013) 3317.
32. D. Hulicova-Jurcakova, M. Kodama, S. Shiraishi, H. Hatori, Z. H. Zhu and G. Q. Lu, *Adv. Funct. Mater.*, 19 (2009) 1800.
33. D. Hulicova, J. Yamashita, Y. Soneda, H. Hatori, and M. Kodama, *Chem. Mater.*, 17 (2005) 1241.
34. Z. S. Wu, W. Ren, L. Xu, F. Li and H. M. Cheng, *ACS Nano*, 5 (2011) 5463.
35. D. L. Fang, Z. D. Chen, X. Liu, Z. F. Wu and C. H. Zheng, *Electrochim. Acta*, 81 (2012) 321.
36. H. D. Liu, J. L. Zhang, D. D. Xu, L. H. Huang, S. Z. Tan and W. J. Mai, *J. Solid State Chem.*, 19 (2015) 135.
37. P. Zhao, W. Li, G. Wang, B. Yu, X. Li, J. Bai and Z. Ren, *J. Alloys Compd.*, 604 (2014) 87.
38. H. L. Guo, P. Su, X. Kang and S. K. Ning, *J. Mater. Chem. A*, 1 (2013) 2248.

© 2018 The Authors. Published by ESG (www.electrochemsci.org). This article is an open access article distributed under the terms and conditions of the Creative Commons Attribution license (<http://creativecommons.org/licenses/by/4.0/>).